NUMERICAL ANALYSIS OF HYDRAULIC TRANSIENTS IN PIPELINE SYSTEMS WITH VARYING BOUNDARY CONDITION USING LAPLACE TRANSFORMATIONS AND FREQUENCY DOMAIN METHOD [+]

Maher Abdul Ameer Khadum [*] Riyad Jassim Telaifih [*] Muayad Nadhim Zemam [**]

Abstract :

This paper foucs on the different between the analytical solution for the variation in hydraulic grade line (HGL). Basic fluid equations solved either, in the time domain, using classical method of charectaristics (MOC) and compare the results with Laplace transformations method and Frequency domain method. The main diffrence between these methods are, the Frequency domain method depends in the analytical solution on the Fourier series approach, but this approach is not well suiet to the case where the boundary conditions vary during the transient event. A Laplace transform solutoin approach overcomes this difficulity accordingly, the results for the pipeline system having varing demand showen that the Laplace transformation sense to wave pressure accur due to suddenly change in flow rate eather than Frequency domain method. By applying these method firstly on assumed network having suddenly chang in flowrate, then applied the mathematical model on Al-Razaza pumping station that suffers from transient flow due to suddenly change in pumping rate, and assumed this practical application to this study. Normalized hypebolic governing equations for apressur transient in a pipeline with change in demand are derived, where the discontinuity induced by a variations in demand by using a delta function. The effects of the change in demand on pipeline system transients induced by a pulse boundary perturbation and continuously changing boundary perturbation are invistigated in detail.

التحليل العددي للجريان الانتقالي في شبكات الانابيب ذات التصريف المتغير باستخدام تحويلات لابلاس وطريقة المدى الترددي

ماهر عبد الله أمير كاظم رياض جاسم طلفاح مؤيد كاظم زمام

المستخلص :

في هذا البحث تم ايضاح الفرق بين التحليل العددي لحالة التغير الحاصلة في خط الانحدار الهيدروليكي بسبب حدوث الجريان الانتقالي. استخدمت في التحليلال المعادلات الاساسية للهيدروليك حيث استخدمت الطريقة التقليدية التي تعتمد في تحليلها المدى الزمني والتي اكثرها شيوعا طريقة الخواص ومقارنة النتائج مع طريقتين الاولى تعتمد

[+] **Received on 22/1/2013 , Accepted on 7/5/2014**

[*] **Lecturer / Technical College / Musayab**

[**] **Assistant Lecturer / Foundation of Technical Education**

تحويلات لابلاس في التحليل والثانية طريقة المدى الترددي وتعتمد تحويلات فورير. تمت دراسة وتحليل موجة الضغط لشبكة مفترضة يتغير فيها التصريف بشكل مفاجئ ثم طبق الموديل الرياضي على محطة ضخ الرزازة التي تعاني من ظاهرة حدوث الجريان الانتقالي ايضا بسبب التغير الفجائي للتصريف واعتبرت تطبيق عملي حي للبحث. لوحظ ان الطريقة التي تعتمد تحويلات لابلاس اكثر تطابق وملائمة عندما تكون الشبكة ذات تصريف متغير من الطريقة التي تعتمد تحويلات فورير حيث ان الاخيرة لا تتحسس كثيرا بالتغيرالفجائي الحاصل للتصريف في الشبكة. تم معالجة المعادلات التي تحكم خاصية الجريان الانتقالي عندما تحصل زيادة مفاجئة للتصريف بسبب دخول مضخات اضافية على الشبكة رياضيا وذلك باستخدام دالة سميت دلتا. تاثيرات التغير في الطلب على منظومات الانابيب تم استنتاجها باستخدام موجات اضطراب محددة واضطرابات متغيرة بشكل متواصل وتم تحليلها بشكل تفصيلي.

1- Introduction :

Hydraulic transients are the time-varying phenomena that follow when the equilibrium of steady flow in a system is disturbed by a change of fiow that occurs over a relatively short time period. The pipe flow and pressure transients can be described by a set of non-linear hyperbolic equations derived from the conservation of mass and Newton's seconed law of motion (conservation of linear –momentom). A closed-form solution for these equations is impossible due to the non-linearity of the momentum equation. A number of methods have been developed to solve these equations analytically where the non-linear term is either neglected [1] or linearized [2,3], and numerically using the method of chacteristics (MOC) and other numerical methods [3,4]. Predominately, transient pipe flows are studied using one-dimensional models assuming a uniform velocity profile. The neglected two-dimensional or three dimensional effects are normally approximated by unsteady-friction models [5,6] with reasonable success.

2- Theoretical analysis :

2-1- Development of the Characteristic Equations :

Neglecting the spatial variation of (V) and (P) whenever both space- and time-varying terms appear in the same equation, in general, the spatial variations are much less significant in determining the solution behavior than the time-varying terms. Then we have two independent partial differential equations [7]

$$\frac{\partial V}{\partial t}+\frac{1}{\rho}\frac{\partial p}{\partial s}+g\frac{dz}{ds}+\frac{f}{2D}V|V|=0 \qquad \text{---------- 1}$$

$$a^2\frac{\partial V}{\partial s}+\frac{1}{\rho}\frac{\partial p}{\partial t}=0 \qquad \text{---------- 2}$$

Using ***l*** as a constant linear scale factor, sometimes called a Lagrange multiplier, one possible combination is

$$\lambda\left(\frac{\partial V}{\partial t}+\frac{1}{\rho}\frac{\partial p}{\partial s}+g\frac{dz}{ds}+\frac{f}{2D}V|V|\right)+\left(a^2\frac{\partial V}{\partial s}+\frac{1}{\rho}\frac{\partial p}{\partial t}\right)=0 \quad \text{---------- 3}$$

Regrouping terms,

$$\left(\lambda\frac{\partial V}{\partial t}+a^2\frac{\partial V}{\partial s}\right)+\left(\frac{1}{\rho}\frac{\partial p}{\partial t}+\frac{\lambda}{\rho}\frac{\partial p}{\partial s}\right)+\lambda g\frac{dz}{ds}+\frac{\lambda f}{2D}V|V|=0 \quad \text{---------- 4}$$

After restrictive conditions on the independent variables in each equations, the two partial differential equations replaced by two pair of ordinary differential equations, the new form of Eqs.(3, 4) is now

$$\frac{dV}{dt}-\frac{g}{a}\frac{dH}{dt}+\frac{f}{2D}V|V|=0 \quad \text{only when} \quad \frac{ds}{dt}=-a \quad \text{---------- 5}$$

$$\frac{dV}{dt}-\frac{g}{a}\frac{dH}{dt}+\frac{f}{2D}V|V|=0 \quad \text{only when} \quad \frac{ds}{dt}=-a \quad \text{---------- 6}$$

2-1-1 The Finite Difference Representation :

In computer manipulations, the Eqs.(5, 6) having new forms, in finite difference form, Eq.(8) becomes

$$\frac{V_P-V_{Le}}{t_P-0}+\frac{g}{a}\frac{H_P-H_{Le}}{t_P-0}+\frac{f}{2D}V_{Le}|V_{Le}|=0 \quad \text{---------- 7}$$

And Eq.(9) becomes

$$\frac{V_P-V_{Ri}}{t_P-0}-\frac{g}{a}\frac{H_P-H_{Ri}}{t_P-0}+\frac{f}{2D}V_{Ri}|V_{Ri}|=0 \quad \text{---------- 8}$$

The analysis will apply to more than the first time interval, accordingly the term $(t_p - 0)$ replaced with (Δt) then the new form gives

$$C^+:\ (V_P-V_{Le})+\frac{g}{a}(H_P-H_{Le})+\frac{f\Delta t}{2D}V_{Le}|V_{Le}|=0 \quad \text{---------- 9}$$

And

$$C^-:\ (V_P-V_{Ri})-\frac{g}{a}(H_P-H_{Ri})+\frac{f\Delta t}{2D}V_{Ri}|V_{Ri}|=0 \quad \text{---------- 10}$$

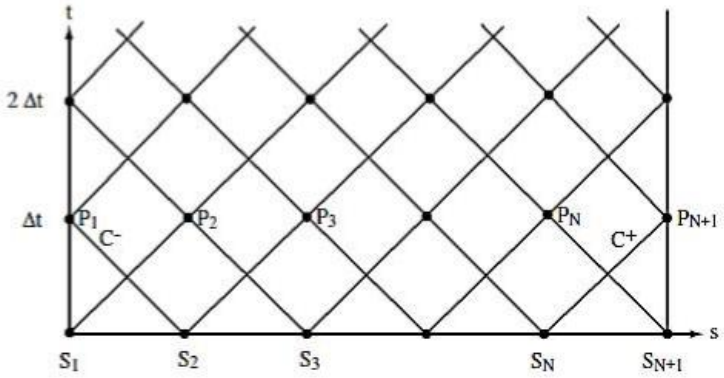

Figure (1): The characteristic grid for a single pipe

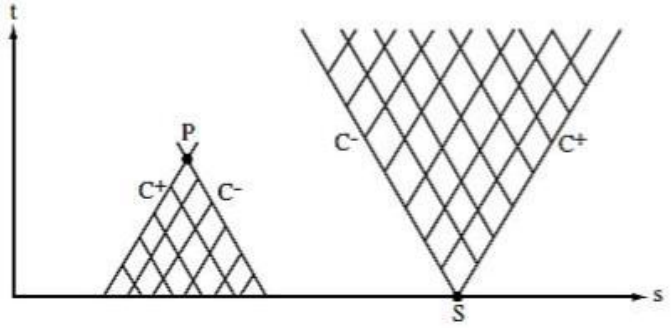

Figure (2): Disturbance propagation in the *s-t* plane

2-1-2 Setting Up the Numerical Procedure :

The values of (*H*) and (*V*) at the ends of the pipe were determined by using boundary conditions. Now we will arrange the solution procedure so it can be conveniently implemented on the computer.

By developing a pair of equations to find (H) and (V) at the interior points (points 2 through N). Solving Eqs.(9, 10) simultaneously to obtain

$$V_P = \frac{1}{2}\left[\left(V_{Le} + V_{Ri}\right) + \frac{g}{a}\left(H_{Le} - H_{Ri}\right) - \frac{f\Delta t}{2D}\left(V_{Le}\left|V_{Le}\right| + V_{Ri}\left|V_{Ri}\right|\right)\right] \quad \text{---------- 11}$$

$$H_P = \frac{1}{2}\left[\frac{a}{g}\left(V_{Le} - V_{Ri}\right) + \left(H_{Le} + H_{Ri}\right) - \frac{a}{g}\frac{f\Delta t}{2D}\left(V_{Le}\left|V_{Le}\right| - V_{Ri}\left|V_{Ri}\right|\right)\right] \quad \text{---------- 12}$$

2-1-3 Constant speed pump boundary condition (upstream end of pipe) :

This boundary condition offers the added complexity of having both (H_{P1} and V_{p1}) in the boundary condition. Consequently the boundary equation must be solved simultaneously with Eq.(12) to produce equations for ($H_{p1}$and V_{p1}) .
The pump boundary condition must be represents by simplest approach that is reasonably general is to represent the pump discharge characteristics by a quadratic equation of the form [7]

$$h_p = A_p' Q^2 + B_p' Q + C_p' \qquad \text{---------- 13}$$

In which (Q) is the pump discharge and(h_p) is the head increases across the pump. These variables are not identical to those in the (C^-) equation, so some adjustments on it by replace (Q) with (V_{P1}) and (h_p) with (H_{P1}– H_{sump}). Incorporating (H_{sump}) into (C_P') and (A) into (A_P') and (B_P') lead to

$$H_{P_1} = A_p V_{P_1}^2 + B_p V_{P_1} + C_p \qquad \text{---------- 14}$$

Eq.(14) is solved simultaneously with the (C^-) characteristic equation, Eq.(12), the elimination of (H_{P1}) leads to the following equation for (V_{P1});

$$V_{P_1} - V_2 - \frac{g}{a}\left(A_p V_{P_1}^2 + B_p V_{P_1} + C_p\right) + \frac{g}{a} H_2 + \frac{f\Delta t}{2D} V_2 |V_2| = 0 \qquad \text{---------- 15}$$

Rearranging,

$$\left(\frac{g}{a} A_p\right) V_{P_1}^2 + \left(\frac{g}{a} B_p - 1\right) V_{P_1} + \left(V_2 + \frac{g}{a} C_p - \frac{g}{a} H_2 - \frac{f\Delta t}{2D} V_2 |V_2|\right) = 0 \qquad \text{---------- 16}$$

This quadratic equation can now be solved for (V_{P1}). then a back substitution into Eq.(14) will yield (H_{P1}).

2-2 Solution Based on the Initial Conditions, Fourier Expansion Procedure :

By linearizing the governing equation for transients in a pipeline with varying demand, the equation having a form [2]

$$\frac{\partial^2 h^*}{\partial x^{*2}} = \frac{\partial^2 h^*}{\partial t^{*2}} + [2R + F_L \delta(x^* - x_L^*)] \frac{\partial h^*}{\partial t^*} \qquad \text{---------- 17}$$

Where ($x^* = x/L$ = dimensionless distance), $t^* = t / (L/a)$ = the dimensionless time, L = pipeline length, a = wave speed, $h^* = (H - H_0) / H_1$ = the dimensionless head of the transient, H= transient head, H_0= steady state head, H_1= a reference head in a pipe, $R = fLQ_o/2DAa$

=resistance term, Q_o= steady state flow rate, f= Darcy-Weisbach factor, D= pipe diameter, A= pipe cross section area, $F_i = C_d A_L a / A\sqrt{2Gh_{Lo}}$ = intake parameter, $C_d A_L$ =effective intake area, H_{Lo} =steady state head at the intake. $\delta(x^* - x_L^*)$ = Dirac delta function and $x_L^* = x_L/L$ = dimensionless intake function.

For the pipeline with constant head, the boundary conditions are given by

$$h^*(0,t^*) = 0 \text{ and } h^*(1,t^*) = 0 \qquad \text{---------- 18}$$

And the initial conditions of the pipeline transients may be defined as

$$h^*(x^*,\ 0) = a_{IC}(x^*) \text{ and } \frac{\partial h^*(x^*,0)}{\partial t^*} = b_{IC}(x^*) \qquad \text{---------- 19}$$

Is the flow out induced damping factor for harmonic component *(n)*.the Fourier coefficients, A_n and B_n, are

$$A_n = 2\int_0^1 a_{IC}(x^*)\sin(n\pi x^*)dx^* \qquad \text{---------- 20}$$

$$B_n = \frac{2}{n\pi}\int_0^1 b_{IC}(x^*)\sin(n\pi x^*)dx^* + \frac{(R+R_{nL})A_n}{n\pi} \qquad \text{---------- 21}$$

2-3 Solution for time dependent boundary conditions, Laplace transformation procedure :

The solution is based on known initial conditions for the pipeline transient. However, it is more practical to measure the time varying initiation process rather than measure the transient distribution along a pipeline. Due to the limitation of the separation of variables technique in solving partial differential equations with time dependent boundary conditions, a solution considering the time dependent initiation process is given using the Laplace transform method [3].

If a pipeline transient is initiated from a steady state condition by a downstream perturbation process, the governing equation and the corresponding boundary and initial conditions are

$$\text{B.C.} \qquad h^*(0,t^*) = 0 \text{ and } h^*(1,t^*) = f(t^*) \qquad \text{---------- 22}$$

$$\text{I.C.} \qquad h^*(x^*,0) = 0 \text{ and } \frac{\partial h^*(x^*,0)}{\partial t^*} = 0 \qquad \text{---------- 23}$$

In which [$f(t^*)$] = dimensionless head at the downstream end of the pipeline.

3-3-1 Pipeline without change in demand discharge :

For a pipeline without any change in demand, $F_L = 0$, and applying Laplace transforms to gives

$$\frac{\partial^2 \tilde{H}(x^*,s)}{\partial x^{*2}} = [s^2 \tilde{H}(x^*,s) - sh^*(x^*,0) - \frac{\partial h^*(x^*,0)}{\partial t^*}] + 2R[s\tilde{H}(x^*,s) - h^*(x^*,0)] \quad \text{---------- 24}$$

Considering the conditions in Eqs.(22, 23), is expressed as

$$\frac{\partial^2 \tilde{H}(x^*,s)}{\partial x^{*2}} = s^2 \tilde{H}(x^*,s) + 2Rs\tilde{H}(x^*,s) \quad \text{---------- 25}$$

Applying the Laplace transforms in Eq.(25) gives

$$\tilde{H}(0,s) = 0 \text{ , and } \tilde{H}(1,s) = \tilde{F}(s) \quad \text{----------26}$$

In which $\tilde{F}(s) = L\{ f(t^*) \}$ = Laplace transform of $f(t^*)$.
For a frictionless pipe, $R = 0$, and the solution for Eq.(26) is

$$\tilde{H}(x^*,s) = C_1 e^{sx^*} + C_2 e^{-sx^*} \quad \text{---------- 27}$$

Substituting Eq.(26) in Eq.(27) and solving gives

$$C_1 = \frac{\tilde{F}(s)}{e^s - e^{-s}} \text{ , and } C_2 = \frac{-\tilde{F}(s)}{e^s - e^{-s}} \quad \text{---------- 28}$$

Therefore, Eq.(27) can be expressed as

$$\tilde{H}(x^*,s) = \sum_{n=0}^{\infty} [\tilde{F}(s) e^{-s(2n+1-x^*)} - \tilde{F}(s) e^{-s(2n+1+x^*)}] \quad \text{---------- 29}$$

2-3-2 Pipeline with varying demand discharge :

For a pipeline with varying discharge, the pipeline can be considered as two portions divided by the intakes that gives a new demand discharge with a small neighborhood (2ε) as shown in Fig.(3)[3]

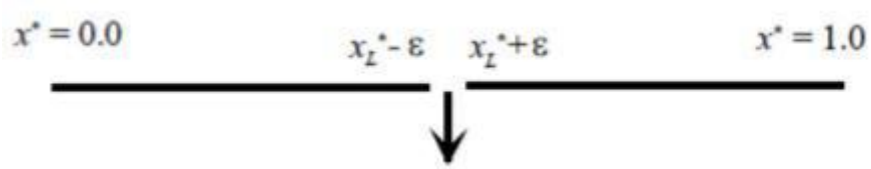

Figure (3): A pipeline with varying discharge

Integrating Eq.(25) over a small neighborhood on either side of the leak gives

$$\int_{x_L^*-\varepsilon}^{x_L^*+\varepsilon}\frac{\partial^2 h^*}{\partial x^{*2}}dx^* = \int_{x_L^*-\varepsilon}^{x_L^*+\varepsilon}\left(\frac{\partial^2 h^*}{\partial t^{*2}}+2R\frac{\partial h^*}{\partial t^*}\right)dx^* + \int_{x_L^*-\varepsilon}^{x_L^*+\varepsilon}F_L\frac{\partial h^*}{\partial t^*}\delta(x^*-x_L^*)dx^* \quad \text{---------- 30}$$

Letting (ε) approach zero, the first integral on the right hand side of Eq.(30) is zero. Thus Eq.(30) becomes

$$\frac{\partial h^*}{\partial x^*}\Bigg|_{x_L^*-\varepsilon}^{x_L^*+\varepsilon} = F_L\frac{\partial h^*(x^*,t)}{\partial t^*}\Bigg|_{x^*=x_L^*} \quad \text{---------- 31}$$

The governing equations for the two frictionless pipe sections on either side of the varying discharge are

$$\frac{\partial^2 h_1^*}{\partial x^{*2}} = \frac{\partial^2 h_1^*}{\partial t^{*2}} \qquad (0 \le x^* < x_L^*, t^* > 0)$$

$$\frac{\partial^2 h_2^*}{\partial x^{*2}} = \frac{\partial^2 h_2^*}{\partial t^{*2}} \qquad (x_L^* < x^* \le 1, t^* > 0) \quad \text{---------- 32}$$

Fig.(4) show the flowchart for surge phenomenon in water distribution systems.

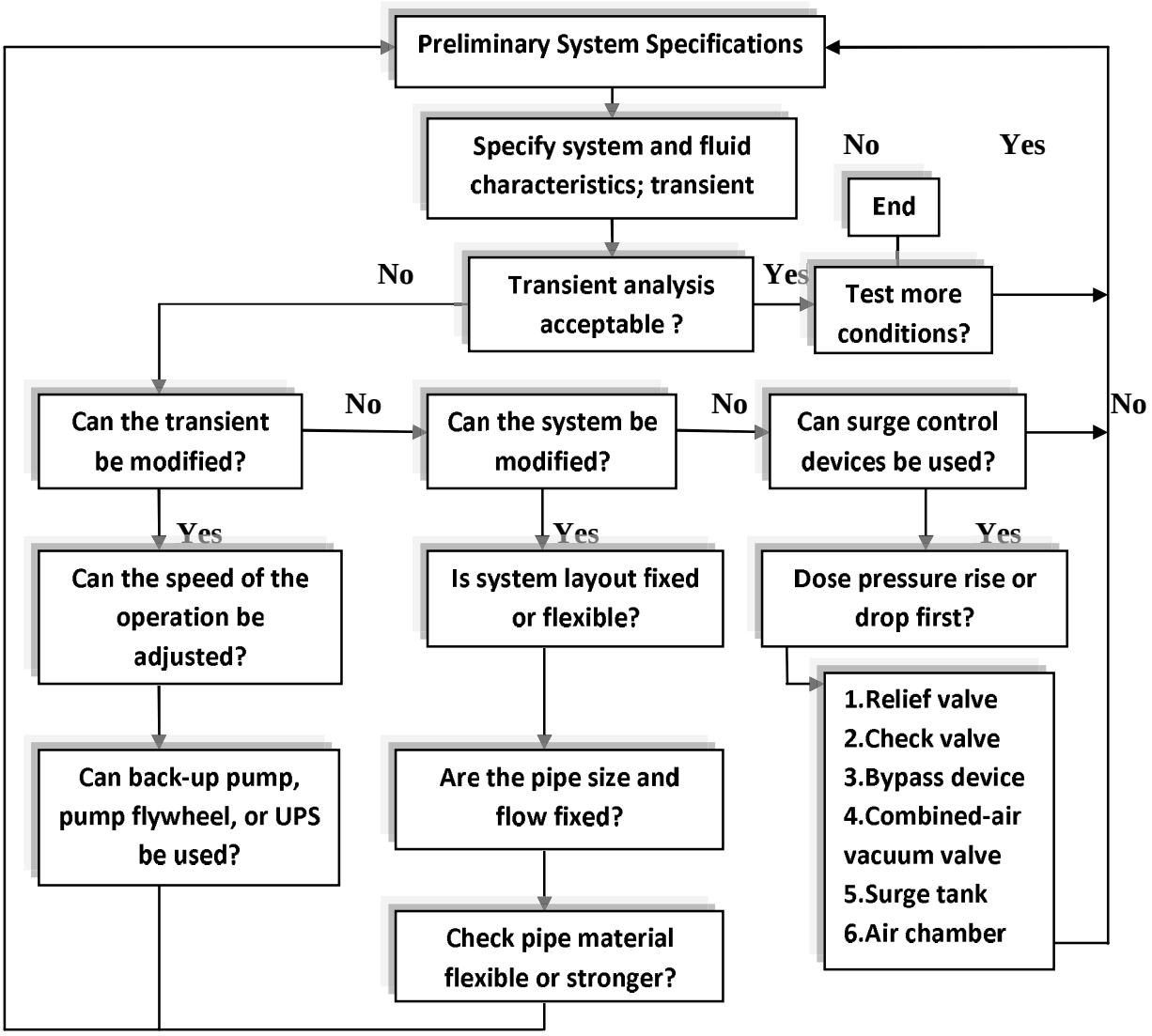

Figure (4): flow chart for transient flow analysis in pipeline systems

3- Hydraulic Applications :

- **Theoretical case study**

The first case study shown in Fig.(5), the simple pipeline system consists from (6) pipes with characteristics shown in table (1), and (6) nodes all data about them shown in table (2), the pump is incorporated into a network and located at one of three reservoirs. The analysis assumes the demand discharge is suddenly increase from (50 gpm) to (790 gpm) due to pump on pipe (6) restart to operate at (20 sec.) and the transient occur downstream the pump, the wave speed is 3000 ft. /s and friction factor (0.02) for all pipes, [7].

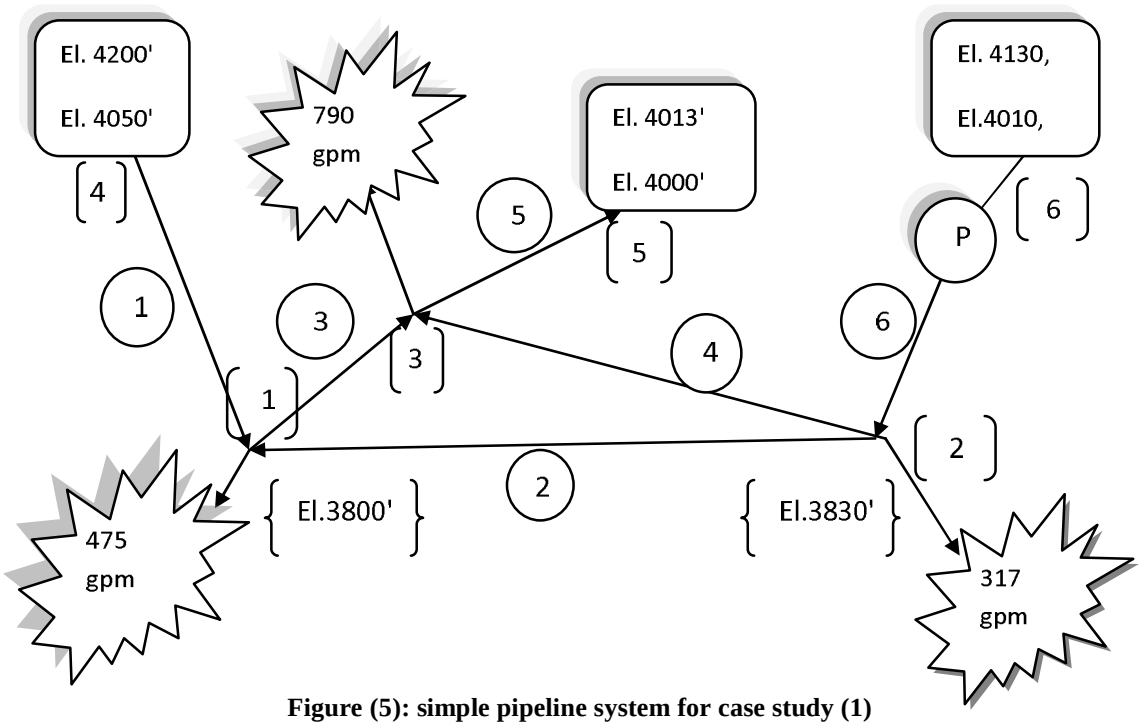

Figure (5): simple pipeline system for case study (1)

Table (1): pipeline data for case study (1)

Pipe No.	Nodes From	to	Length Ft.	Dia. In.	*f*	Q gpm	Vel. Ft/s	H_L ft.
1	4	1	3300	12.0	0.02	340.1	0.96	0.40
2	2	1	8200	8.0	0.02	273.0	1.47	1.91
3	1	3	3300	8.0	0.02	138.1	0.88	0.54
4	2	3	4900	12.0	0.02	1110.0	3.15	3.57
5	3	5	3300	6.0	0.02	458.1	5.20	20.27
6	6	2	2600	14.0	0.02	1700.0	3.54	3.71

Table (2): nodes data for case study (1)

Node	Demand gpm	El. Ft.	Head Ft.	Pressure Psi.	HGL El. Ft.
1	475	3800	398.68	172.76	4198.68
2	317	3830	384.38	166.57	4214.38
3	790	3770	426.89	184.99	4196.89
6	-1700	4010	214.03	92.74	4224.03
4	-340	4050	150.00	65.00	4200.00
5	458	4000	130.00	56.33	4130.00

- **Practical application**

This case study focus on the transient analysis for Al-Razaza pumping station, this station suffering a transient caused by suddenly change in discharge due to operate PS_2 on the same main pipes for PS_1. The original design for this pumping station contains only PS_1 having (5 axial pumps), (4 pumps in service and 1 pump stand by) connects (2 main pipes) with (2 m) diameter and (800 m) long (2 pumps) for each individual pipe, the characteristics for these pumps;[10]

Discharge (Q) = 3.8 m^3/s
Revolution (rpm) =423 rpm
Head (H) =23 m
Power (HP) for the electric motor = 1600 Kw

Due to increasing in the drainage water for Al-Razaza drain, these pumps be not sufficient to occupies this drain especially in winter and spring, this problem being need to solve, the staff in this station installed PS_2 in parallel to the PS_1. The new station contains (12 horizontal pumps), 10 pumps operate and 2 pumps stand by, each 6 pumps connects with collector pipe, each one goes to main pipe then to Al-Razaza lack. The characteristics for these pumps;

Discharge (Q) = 1 m^3/s
Revolution (rpm) = 1200 rpm
Head (H) =21 m
Power (HP) = 340 Kw

When the drainage water rises, PS_2 be operated, here the transient flow start soon and 2 stand pipes having (20 m) height and (3 m) diameter installed one on each of the main pipe at distance (20 m) from axial pumps and (23 m) from horizontal pumps, these stand pipes flooded. The station was tested when this phenomenon being start and the layout suffering transient, the nodal was tested in the downstream of the stand pipes (1). Fig.(6) shown the layout for the whole station, table (3) give all hydraulic pressures for the main pipes when three axial pumps in service with variable numbers of horizontal pumps, the friction factor for the main pipes and collector pipes (0.031), the total rotary moment of inertia of each pump and motor unit is (475 Ib-ft^2), the wave speed for steel pipe (3490 ft/s).

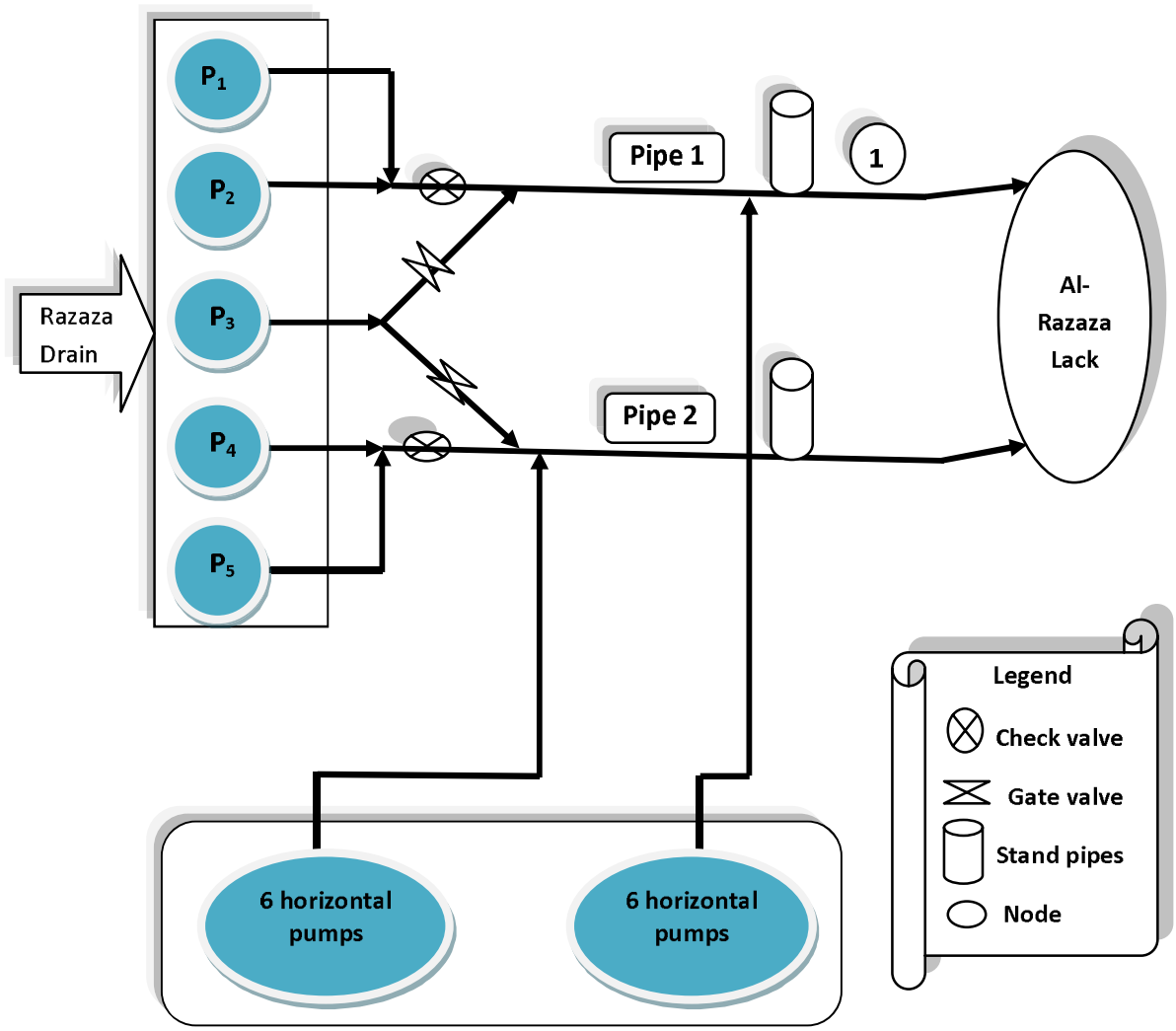

Figure (6): typical layout for Al-Razaza pumping station

Table (3): hydraulic pressures in the main pipes when three axial pumps in the service with variable numbers of horizontal pimps.

No. of horizontal pumps	Pressure on surge tank in pipe 1(m)	Pressure on surge tank in pipe 2(m)	Velocity in pipe 1 (m/s)	Velocity in pipe (m/s)	Discharge in pipe 1(m^3/s)	Discharge in pipe 2(m^3/s)	H_L(m)in1	H_L in 2(m)
1	44.13	44.17	2.20	2.22	6.98	6.97	2.07	2.1
2	44.35	44.35	2.34	2.34	7.35	7.36	2.33	2.3
3	44.57	44.61	2.46	2.48	7.72	7.78	2.54	2.6
4	44.82	44.83	2.59	2.59	8.13	8.14	2.79	2.8
5	45.04	45.08	2.69	2.69	8.45	8.51	3.01	3.0
6	45.28	45.29	2.81	2.81	8.82	8.83	3.25	3.3
7	45.49	45.53	2.90	2.92	9.11	9.17	3.46	3.5
8	45.72	45.73	3.00	3.01	9.43	9.45	3.68	3.7
9	45.91	45.95	3.09	3.10	9.69	9.75	3.78	3.9
10	46.13	46.14	3.18	3.18	9.98	10.01	4.09	4.1

4- Conclusion and Recommendations :

During the observations of the analysis of the three methods used in this research, the method in which depend Laplace transforms in the analysis more accurate in sensing the pressure wave when suddenly change in demand or in other word in pumping rate in network systems. Fig.(7) clearly shown the wave pressure accurse in the assumed network after the suddenly change in flow rate and how the Laplace transforms gives the pressure wave more accurate from the others methods. The same results were obtained when Appling the model on Al-Razaza pumping station that suffering transient flow due to suddenly change in pumping rate, fig.(8) clearly shown this phenomenon.

The recommendations of the research can be summarized as follows

- Analysis of other cases of transient flow, such as more complex networks suffering transients due to air entrainment on fluid.
- Analysis transients due to changes in valve settings, or change within the transmission system, change in storage tank operation.
- Analysis of other network systems having possibility of sudden changes in pressure due to change in temperature or sudden move of hydraulic ram.

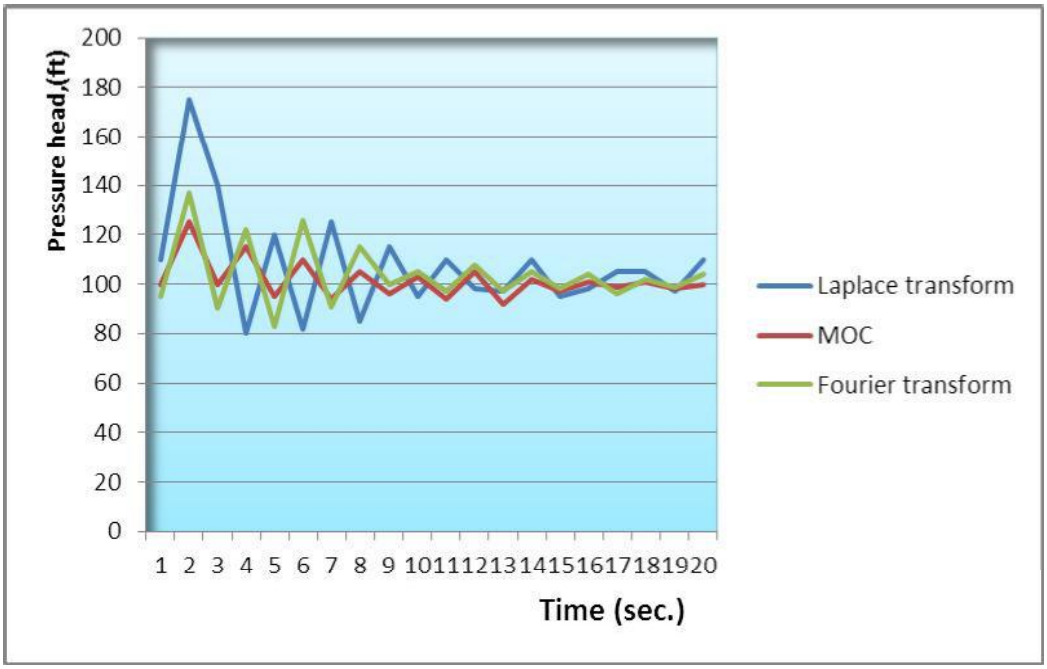

Figure (7): pressure head downstream the pump for case study(1) to all methods.

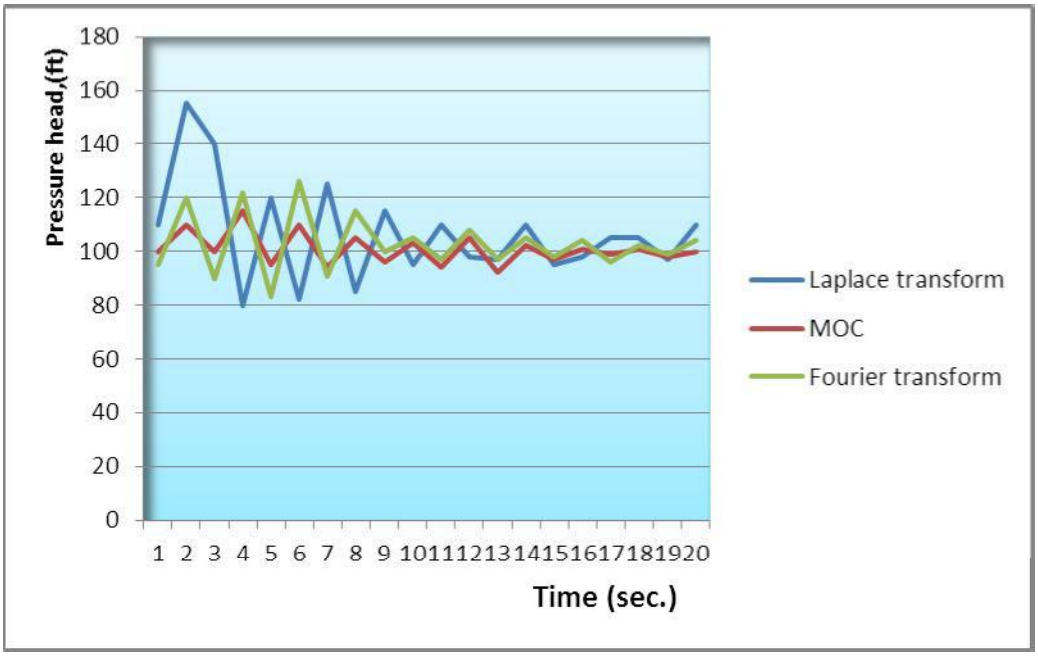

Figure (8), Pressure head down stream of the stand pipe at point (1) on main pipe (1) for Al-Razaza pumping station to all methods.

5- References :

1. Allievi, L. "*Theory of water hammer*" ,Translated by E. E. Halmos. Riccardo Garroni, Rome, 1995.
2. Zielke, W.."*Frequency-dependent friction in transient pipe flow*."Journal of Basic Engineering. ASME, 90, 109-115, 1968.
3. X. Wang, M. F. Lambert and A. R. Simpson, "*Analysis of a Transient in a Pipeline with Leak Using Laplace Transforms*", 14th Australian Fluid Mechanics Conference. 2001.
4. Rich, G. R. "*Water hammer analysis by the Laplace-Mellin transformation*" Transactions of ASE, 67, 361-376, 1985.
5. Chaudhry, M. H."*Applied Hydraulic Transients*", Van Nostrand Reinhold Company, New York, 1987.
6. Wood, F. M."*Application of Heaviside's operational calculus to the solution of problems in water hammer*" Transaction of ASME, 59, 707-713, 1988.
7. Bruce E. Larock, Roland W. Jeppson, Gary Z. Watters." *Hydraulic of Pipeline Systems*," 2000
8. Vardy, A. E., and Hwang, K-L.." *A characteristics model of transient friction in pipes*" Journal of Hydraulic Research, IAHR, 29(5), 669-684, 1991.
9. Brunone, B., Golia, U. M., and Greco, M. " *Modeling of fast transients by numerical methods*" International meeting on hydraulic transients with Colum Separation, IAHR, Valencia, Spain, 201-209, 1991.
10. Al-Razaza pumping station, Directories of water resources for Kerbela governorate.

Nomenclature :

Symbol	Quantity	Unit		Dimension
		SI	English	
A	Cross section area of pipe	m^2	ft^2	$\mathbf{L^2}$
A_n	Fourier coefficients		Dimensionless	
A_P	Polynomial constants		Dimensionless	
a	Wave celerity	m/s	ft/s	**L/t**
a_{IC} (x^*) and b_{IC} (x^*)	Piecewise continuous functions		Dimensionless	
$C_d A_L$	Effective intake area	m^2	ft^2	$\mathbf{L^2}$
D	Pipe diameter	m	ft	**L**
$F_i = C_d A_L a / A\sqrt{2Gh_{Lo}}$	Intake parameter		Dimensionless	
f	Friction factor		Dimensionless	
g	Gravitational acceleration	m/s^2	ft/s^2	$\mathbf{L/t^2}$
H	Transient head	m	ft	**L**
H_0	Steady state head	m	ft	**L**
H_1	Reference head in a pipe	m	ft	**L**
H_{Lo}	Steady state head at the intake	m	ft	**L**
h_p	Pump head	m	ft	**L**
l	Scale factor		Dimensionless	
P	Pressure	Pa	Ib/ft^2	$\mathbf{ML^{-1}t^{-2}}$
Q_o	Steady state flow rate	m^3/s	ft^3/s	$\mathbf{L^3t^{-1}}$
$R = fLQ_o/2DAa$	Resistance term		Dimensionless	
s	Space	m	ft	**L**
$t^* = t / (L/a)$	Dimensionless time		Dimensionless	
$x^* = x/L$	Dimensionless distance		Dimensionless	
V	Average velocity	m/s	ft/s	$\mathbf{Lt^{-1}}$
$x_L^* = x_L/L$	Dimensionless intake function		Dimensionless	
ρ	Mass density	Kg/m^3	Ib/ft^3	$\mathbf{ML^{-3}}$
λ	Lagrange multiplier		Dimensionless	
sub scribt)$_P$	Node value for finite deference			
sub scribt)$_{Le}$	Left value for finite deference			
sub scribt)$_{Ri}$:	Right value for finite deference			
$\delta(x^* - x_L)^*$	Dirac delta function		Dimensionless	
ε	small neighborhood	m	ft	**L**

ENHANCEMENT OF A POWER SYSTEM TRANSIENT STABILITY USING THYRISTOR CONTROLLED SERIES COMPENSATOR TCSC [+]

Naseer M. Yasin [*] **Mustafa M. Al-Eedany** [**]

Abstract:

Thyrirstor Controlled Series Compensator (TCSC) is well known as an effective device for regulating active power flow in a power system. In this paper The TCSC linearized power flow equations, with respect to the firing angle, are incorporated into Newton-Raphson algorithm in a MATLAB written program to investigate the active power flow and transient stability of a five bus and a thirty bus test systems, when a three phase fault occurs near one of the buses. Comparison of the results obtained for the base case when no TCSC is connected and those when it is connected to investigate the effectiveness of the device on both of the active power flow and the transient stability. The power flow was increased by 8.33% and the Critical Clearing Time (CCT) was increased by 6.3% for the 5-bus test system, while for the 30-bus the power flow was increased by 2.55% and the CCT by 0.5%.

تعزيز الاستقرارية العابرة لنظام القدرة باستخدام المعوض المتوالي المسيطر عليه بالثايرستور

نصير مجيد ياسين مصطفى العيداني

المستخلص :

يعرف المعوض المتوالي كجهاز لتنظيم سريان القدرة الفعالة. في هذا البحث تم استخدام معادلات سريان القدرة مع زوايا القدح وبطريقة نيوتن رافسون في برنامج مكتوب بلغة ماتلاب لبحث سريان القدرة الفعالة والاستقرارية العابرة لمنظومة ذات خمسة محطات واخرى ذات ثلاثين محطة عند حدوث خطأ ثلاثي في احد المحطات. تم أجراء مقارنة بين نتائج النظام في حالة وجود المعوض المتوالي وفي حالة عدم وجوده لدراسة تأثيره على سريان القدرة الفعالة والاستقرارية العابرة, وقد كانت نسبة الزيادة في سريان القدرة 8,33٪ وفي زمن الازالة الحرج 6،3٪ بالنسبة للنظام ذو خمسة الواح, وبمقدار2,5٪ للقدرة الفعالة و 0,5٪ لزمن الازالة الحرج بالنسبة للنظام ذو ثلاثين لوح.

1. Introduction :

Monitoring the stability status of a power system in real time has been recognized as a task of primary importance in preventing blackouts. In case of a disturbance leading to transient instability, fast recognition of the potentially dangerous conditions is very crucial for allowing sufficient time to take emergency control actions [1]. Several attempts to develop an effective real-time transient stability indicator have been reported in the literature [1-4].

[+] **Received on 2/1/2013 , Accepted on 13/5/2014**

[*] **Assistant Lecturer / Electrical and Electronic Technical College**

[**] **Assistant Prof. / College of Engineering / University of Basrah**

The transient stability of power systems is associated with the ability of the generators to remain in synchronism after a severe disturbance. It depends upon the severity of the contingency and the initial operating state of the power systems [5]. Here the term contingency, also called disturbance or fault, indicates an event like three-phase short circuit in the grid that will cause large changes in power system [6]. Operating power system will first encounter the hurdle of transient stability before apparatuses thermal limits [7]. This is particularly true for many power systems nowadays as they are being forced to squeeze the last drop from the infrastructure due to increasing demands but limited electrical apparatus capacity. In such a circumstance when a contingency occurred in the electrical network, the power system is likely to lose stability, or may be even worse to trigger large scale blackouts [8].
In order to avoid catastrophic outages, power utilities resort to various planning, protection and control schemes. Preventive control is summoned up when the power system is still in normal status. It encompasses many types of control actions, including generation rescheduling, load curtailment and network switching reactive compensation [9,10]. Those preventive control actions reallocate power system operating state so that it can guarantee satisfactory behavior after a contingency occurred in the grid.
Time-domain simulation is an effective tool for power system plan, design and operation [11].Transient stability assessment (TSA) is the study of synchronism of generator rotor angles after being subjected to a disturbance [5]. This is also known as rotor angle stability. The real time TSA is important to the power system security and efficient operation. Otherwise essential control actions could be delayed; which in turn could trigger a large scale blackout. Further, real time TSA will avoid any unnecessary control commands to ensure the minimum impact on the grid.
The conventional transient stability measure of a system's robustness to withstand a large disturbance is its corresponding CCT which is the maximum time duration for which the disturbance may act without the system losing its capability to recover a steady-state which means stable operation [12].
In the late 1980s, the Electric Power Research Institute (EPRI) formulated the vision of the Flexible AC Transmission Systems (FACTS) in which various power-electronics based controllers regulate power flow and transmission voltage and mitigate dynamic disturbances. Fast development of power electronic technology has made FACTS promising solution of future power system. FACTS controllers such as Static Synchronous Compensator (STATCOM), Static VAR Compensator (SVC), Thyristor Controlled Series Compensator (TCSC), Static Synchronous Series Compensator (SSSC) and Unified Power Flow controller (UPFC) are able to change the network parameters in a fast and effective way in order to achieve better system performance [13]. These controllers are used for enhancing dynamic performance of power systems in terms of voltage/angle stability while improving the power transfer capability and voltage profile in steady-state conditions [14].
TCSC is a series compensator, which allows rapid and continuous changes of transmission impedance, controlling power flow in the line and improving system stability [15]. It uses high-current power electronic devices to control the power flow of a transmission system. FACTS devices are very effective and capable of increasing the power transfer capability of a line, if the thermal limit permits, while maintaining the same degree of stability [16].

2. Modeling of TCSC :

Figure (1) shows the TCSC module connected in series with a transmission line. TCSCs vary the electrical length of the compensated transmission line with little delay. This characteristic enables the TCSC to be used to provide fast active power flow regulation. It also increases the stability margin of the system.

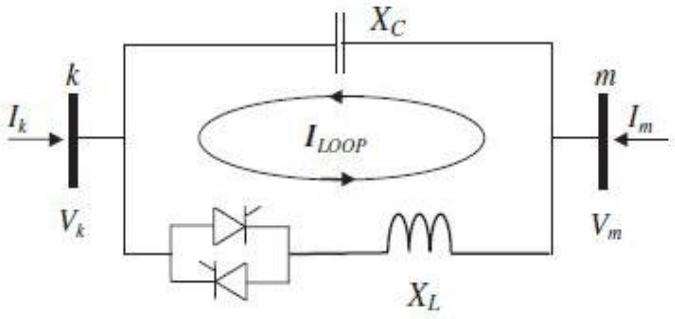

Figure (1): Thyristor-controlled series capacitor (TCSC) equivalent circuit

A nonlinear equivalent impedance expression for the fundamental frequency [17] is:

$$X_{tcsc} = -X_c + C_1\{2(\pi-\alpha) + \sin[2(\pi-\alpha)]\} + C_2 cos^2(\pi-\alpha)\{\bar{\omega}\tan[\bar{\omega}(\pi-\alpha)] - tan(\pi-\alpha)\} \quad \text{----------1}$$

Where:

$$C_1 = X_c + X_l/\pi \quad \text{----------2}$$

$$C_2 = -4X_{lc}{}^2/\pi X_l \quad \text{----------3}$$

$$X_{lc} = X_c - X_l / X_c - X_l \quad \text{----------4}$$

$$\bar{\omega} = (X_c/X_l)^{½} \quad \text{----------5}$$

The Thyristor Controlled Reactor TCR achieves its fundamental frequency operating state at the expense of generating harmonic currents, which are a function of the thyristor conduction angle. Nevertheless, contrary to the Static Var Compensator SVC application where the harmonic currents generated by the TCR tend to escape towards the network, in the TCSC application the TCR harmonic currents are trapped inside the TCSC because of the low impedance of the capacitor compared with the network equivalent impedance [17]. Since the explicit information about the TCSC impedance-firing angle is available, good initial conditions are easily selected, hence preventing power flow iterative process from entering the non-operative regions owing to the presence of resonant bands as shown in Figure (2).

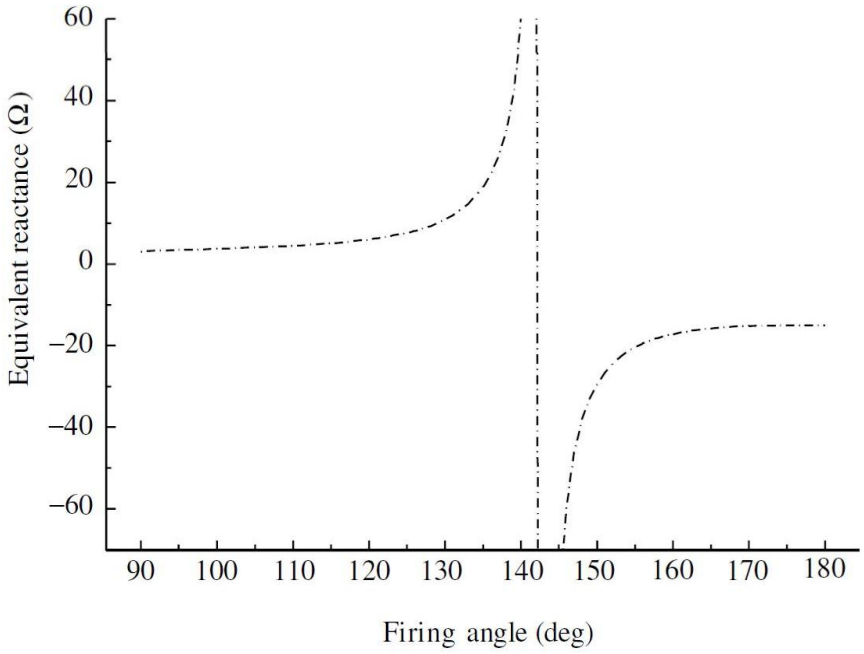

Figure (2): TCSC fundamental frequency impedance

The performance of the TCSC mathematical model is affected by the number of internal resonant points exhibited by the TCSC in the range π to 2π. The resonant points (poles) are determined by the following expression [17].

$$\alpha_{tcsc} = \pi \left[1 - \frac{(2n-1)\omega\sqrt{LC}}{2}\right] \text{----------6}$$

Where n=1, 2, 3…

The pole defines the transition from the inductive to the capacitive region, as the firing angle increases. For the case when the TCSC controls active power flowing from bus k to bus m, at a specified value.

$$P_k = V_k\, V_m B_{km}\ \sin(\delta_k - \delta_m) \text{----------7}$$

$$Q_k = -V_k{}^2 B_{kk} - V_k\, V_m\, B_{km} \cos(\delta_k - V_m) \text{----------8}$$

For the powers at bus m, exchange the subscripts k and m.

The set of linearized power flow equations is:

$$\begin{vmatrix} \Delta P_k \\ \Delta P_m \\ \Delta Q_k \\ \Delta Q_m \\ \Delta P_{km} \end{vmatrix} = \begin{vmatrix} \partial P_k/\partial \delta_k & \partial P_k/\partial \delta_m & \partial P_k/\partial V_k & \partial P_k/\partial V_m & \partial P_k/\partial \alpha \\ \partial P_m/\partial \delta_k & \partial P_m/\partial \delta_m & \partial P_m/\partial V_k & \partial P_m/\partial V_m & \partial P_m/\partial \alpha \\ \partial Q_k/\partial \delta_k & \partial Q_k/\partial \delta_m & \partial Q_k/\partial V_k & \partial Q_k/\partial V_m & \partial Q_k/\partial \alpha \\ \partial Q_m/\partial \delta_k & \partial Q_m/\partial \delta_m & \partial Q_m/\partial V_k & \partial Q_m/\partial V_m & \partial Q_m/\partial \alpha \\ \partial P_{km}/\partial \delta_k & \partial P_{km}/\partial \delta_m & \partial P_{km}/\partial V_k & \partial P_{km}/\partial V_m & \partial P_{km}/\partial \alpha \end{vmatrix} \begin{vmatrix} \Delta \delta_k \\ \Delta \delta_m \\ \Delta V_k \\ \Delta V_m \\ \Delta \alpha \end{vmatrix} \text{-------9}$$

The elements of the added row and column are

$$\partial P_k/\partial \alpha = -V_k V_m B_{tcsc}{}^2 \sin(\delta_k - \delta_m)\, \partial X_{tcsc}/\partial \alpha \text{----------10}$$

$$\partial Q_k/\partial \alpha = (-V_k{}^2 + V_k V_m cos(\delta_k - \delta_m)) B_{tcsc}{}^2\, \partial X_{tcsc}/\partial \alpha \text{----------11}$$

$$\partial X_{tcsc}/\partial \alpha = -2C_1[1+\cos(2\alpha)+C_2\sin(2\alpha)\{\bar{\omega}\tan[\bar{\omega}(\pi-\alpha)]+\tan\alpha\}+C_2\{\bar{\omega}^2\cos^2(\pi-\alpha)/\cos^2[\bar{\omega}(\pi-\alpha)]-1\} \text{----------12}$$

$$B_{kk} = -B_{km} = B_{tcsc} \text{----------13}$$

$$\Delta P_{km} = P_{kmreg} - P_{kmcal} \text{----------14}$$

is the difference between the specified active power (required active power flow in the TCSC branch) and the calculated active power.

The firing angle is updated according to

$$\alpha(i+1) = \alpha(i) + \Delta\alpha \text{----------15}$$

Where $\Delta\alpha$ is the incremental change in the TCSC's firing angle and i is the ith iteration.

3. Program Structure:

After reading the line and bus data for the power system, the MATLAB written program starts by forming the bus admittance, then using Newton Raphson method, it calculates the active and reactive power of the slack bus, the voltages and angles of each load bus. Then the stability program calculates the new bus admittance during fault, and the post fault admittance. The solution of the differential power equations is solved using Runge-Kutta method to simulate the variation of power angle with time. Figure (3) shows the flow chart of the program.

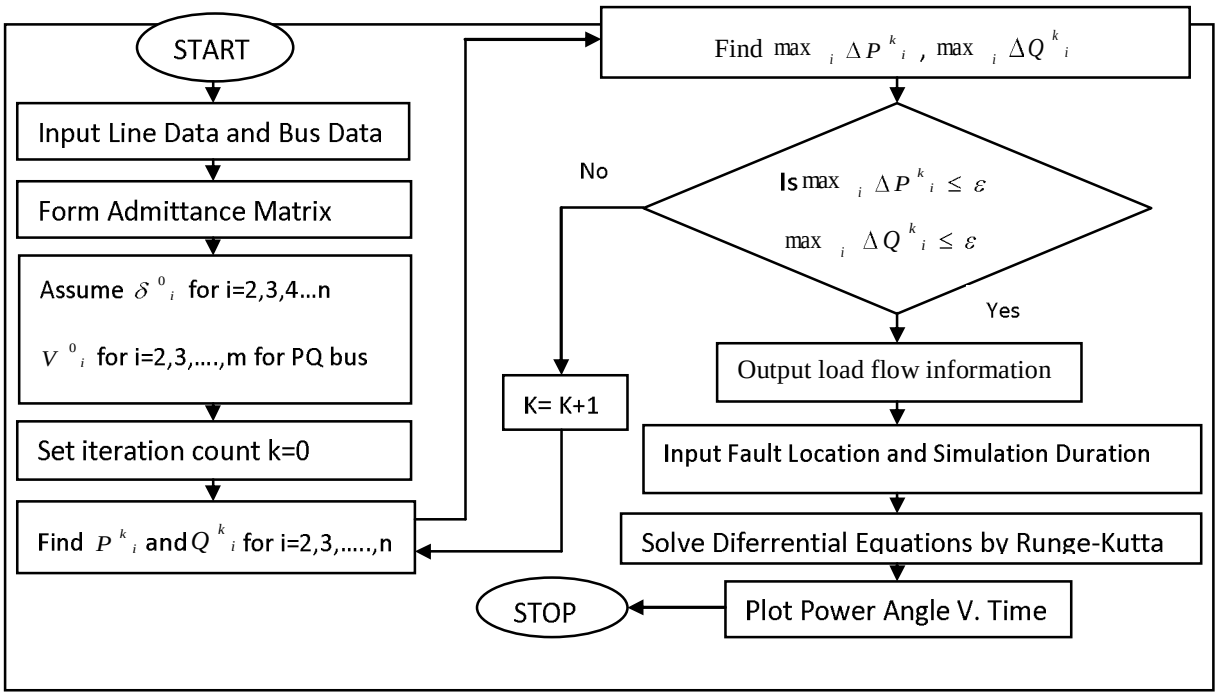

Figure (3): Flow chart of load flow and transient stability program

4. Simulation and results:

The IEEE 5-bus system shown in Figure (4) is used to test the effectiveness of connecting the TCSC device between bus3 and bus4, the data of this system can be found in [17].

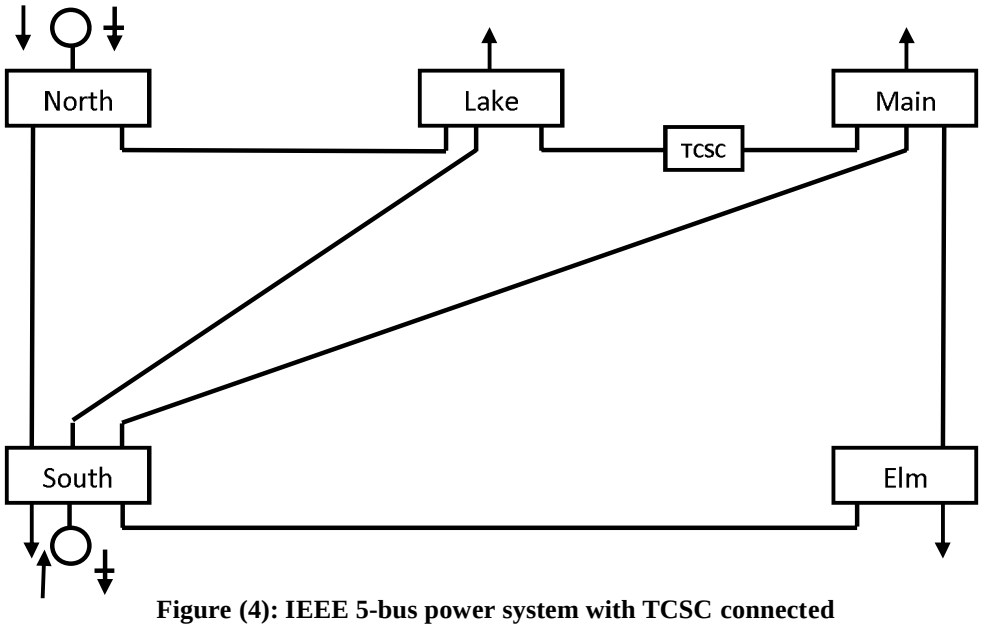

Figure (4): IEEE 5-bus power system with TCSC connected

Using Newton-Raphson method, load flow and power flow results of the system without the TCSC connected are shown Table (1&2).

Table (1): Load flow results of 5-bus system without TCSC connected

Power Flow Solution by Newton-Raphson Method						
Maximum Power Mismatch = 2.84495e-015						
No. of Iterations = 5						
Bus	Voltage	Angle	------Load------		---Generation--	
No.	Mag.	Degree	P(MW)	Q(MVAR)	P(MW)	Q(MVAR)
1	1.060	0.000	0.000	0.000	131.122	90.816
2	1.000	-2.061	20.000	10.000	40.000	-61.593
3	0.987	-4.637	45.000	15.000	0.000	0.000
4	0.984	-4.957	40.000	5.000	0.000	0.000
5	0.972	-5.765	60.000	10.000	0.000	0.000
Total			165.000	40.000	171.122	29.223

Table (2): Power flow results of 5-bus system without TCSC connected

Line Flow and Losses						
--Line--		Power at bus & line flow			--Line loss--	
From	To	P(MW)	Q(MVAR)	S(MVA)	P(MW)	Q(MVAR)
1	1	131.122	90.816	159.501		
1	2	89.331	73.995	115.997	2.486	1.087
1	3	41.791	16.820	45.049	1.518	-0.692
2	2	20.000	-71.593	74.334		
2	1	-86.846	-72.908	113.392	2.486	1.087
2	3	24.473	-2.518	24.602	0.360	-2.871
2	4	27.713	-1.724	27.767	0.461	-2.554
2	5	54.660	5.558	54.942	1.215	0.729
3	3	-45.000	-15.000	47.434		
3	1	-40.273	-17.513	43.916	1.518	-0.692
3	2	-24.113	-0.352	24.116	0.360	-2.871
3	4	**19.386**	2.865	19.597	0.040	-1.823
4	4	-40.000	-5.000	40.311		
4	2	-27.252	-0.831	27.265	0.461	-2.554
4	3	-19.346	-4.688	19.906	0.040	-1.823
4	5	6.598	0.518	6.619	0.043	-4.652
5	5	-60.000	-10.000	60.828		
5	2	-53.445	-4.829	53.663	1.215	0.729
5	4	-6.555	-5.171	8.349	0.043	-4.652
Total loss					6.122	-10.777

It is required to enhance the power flow from bus3 to bus4 to a higher value of 21MW instead of 19.386MW, so that the system is able to cope with a bigger load. This is done by creating a new bus between bus3 and bus4 namely bus6 and connecting the TCSC between bus3 and

bus6. The new system manages to achieve this task and maintains active power flow at the specified value in six iterations with a final firing angle of 148.4675˚, the load flow and the power flow with the TCSC connected are shown Table (3) and Table (4).

Table (3): Load flow results of 5-bus system with TCSC connected

Power Flow Solution by Newton-Raphson Method						
Maximum Power Mismatch = 1.43774e-014						
No. of Iterations = 6						
Bus	Voltage	Angle	------Load------		---Generation---	
No.	Mag.	Degree	P(MW)	Q(MVAR)	P(MW)	Q(MVAR)
1	1.060	0.000	0.000	0.000	131.127	90.937
2	1.000	-2.038	20.000	10.000	40.000	-61.801
3	0.987	-4.727	45.000	15.000	0.000	0.000
4	0.984	-4.811	40.000	5.000	0.000	0.000
5	0.972	-5.701	60.000	10.000	0.000	0.000
6	0.988	-4.461	0.000	0.000	0.000	0.000
Total			165.000	40.000	171.127	29.136

Table (4): Power flow results of 5-bus system with TCSC connected

Line Flow and Losses						
--Line--		Power at bus & line flow			--Line loss--	
From	To	P(MW)	Q(MVAR)	S(MVA)	P(MW)	Q(MVAR)
1	1	131.127	90.937	159.574		
1	2	88.680	74.187	115.619	2.470	1.041
1	3	42.448	16.750	45.633	1.555	-0.579
2	2	20.000	-71.801	74.534		
2	1	-86.209	-73.146	113.059	2.470	1.041
2	3	25.498	-2.694	25.640	0.390	-2.777
2	4	26.605	-1.567	26.651	0.425	-2.664
2	5	54.106	5.606	54.396	1.191	0.657
3	3	-45.000	-15.000	47.434		
3	1	-40.892	-17.329	44.412	1.555	-0.579
3	2	-25.108	-0.083	25.108	0.390	-2.777
3	6	21.000	2.412	21.138	-0.000	-0.099
4	4	-40.000	-5.000	40.311		
4	2	-26.180	-1.097	26.203	0.425	-2.664
4	6	-20.954	-4.316	21.393	0.046	-1.805
4	5	7.134	0.413	7.146	0.049	-4.638
5	5	-60.000	-10.000	60.828		
5	2	-52.915	-4.949	53.146	1.191	0.657
5	4	-7.085	-5.051	8.701	0.049	-4.638
6	6	0.000	0.000	0.000		
6	3	-21.000	-2.511	21.150	-0.000	-0.099
6	4	21.000	2.511	21.150	0.046	-1.805
Total loss					6.127	-10.864

To show that the new system's transient stability has been enhanced, a three phase fault is created near bus1 at transmission line (1-2), and cleared by the removal of the same transmission line for both the base case and the new system. A plot of the power angle difference between the two generators at bus1 (slack bus) and bus2 (voltage controlled bus) which means ($\delta 2$-$\delta 1$) is shown in Figure (5). The swing curve shows that the power system is stable for clearing time Tc=0.397sec. and loses stability for Tc=0.398sec, therefore the critical clearing time is CCT=0.397sec.

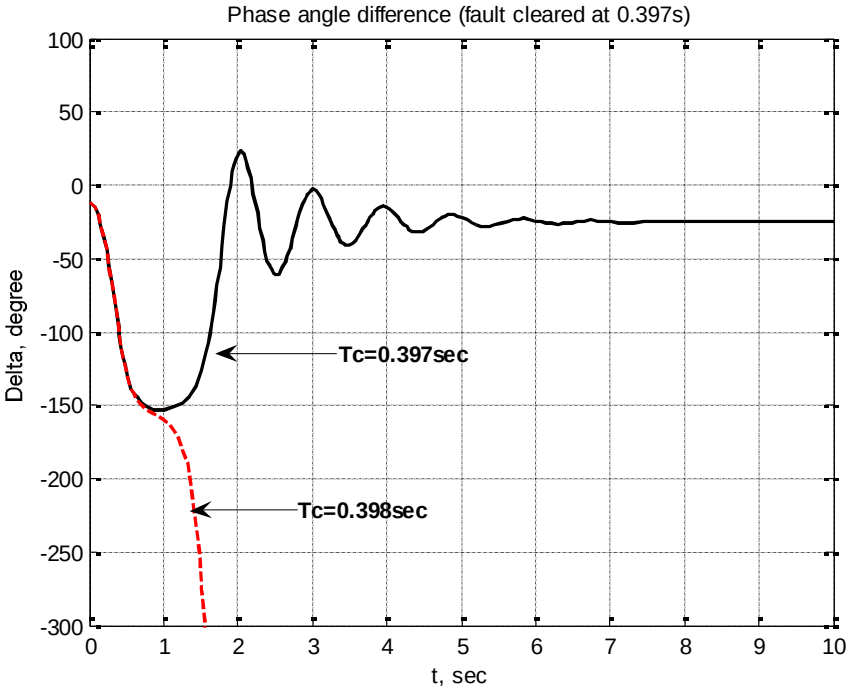

Figure (5): Power angle curve for IEEE5-bus test system, Fault at T.L. 1-2, Without TCSC

To test weather the stability has been enhanced, the same fault that was created near bus1 at transmission line 1-2 is simulated and the power angle curve is plotted as shown in Figure (6). The system is considered to be stable for CCT=0.399sec, and has acquired an increase of 0.5% compared with the base case.

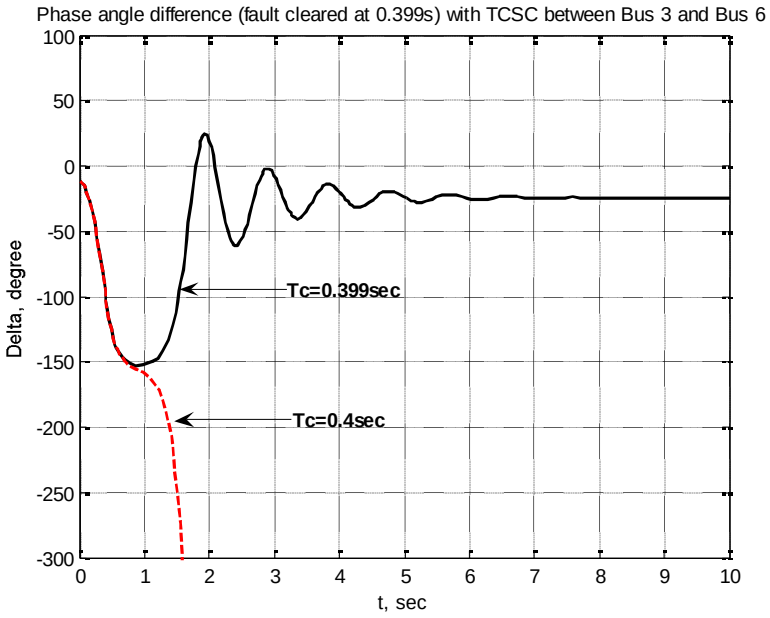

Figure (6): Power angle curve for IEEE5-bus test system, fault at T.L. 1-2 With TCSC included

The other test system is the IEEE 30-bus system, the single line diagram of which is shown in Figure (7) is implemented to evaluate the effectiveness of the TCSC model. The data of which can be found in [18].

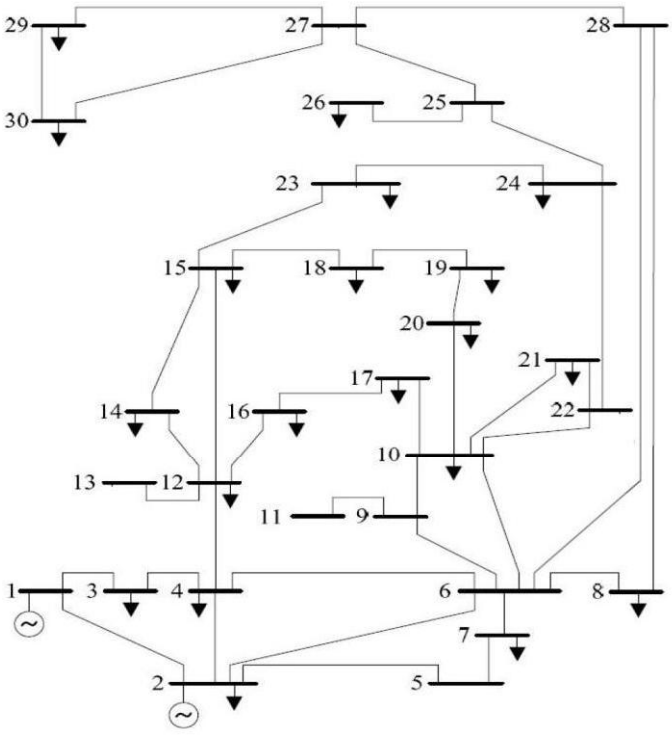

Figure (7): IEEE 30-bus power system

By using Newton-Raphson method, the power flow results of the system without the TCSC are shown in Table (5) below (for bus3 only).

Table (5): Power flow results of 30-bus system without TCSC connected
For bus 3 only

Line Flow and Losses						
--Line--		Power at bus & line flow			--Line loss--	
From	To	P(MW)	Q(MVA)	S(MVA)	P(MW)	Q(MVA)
1	1	260.999	-17.021	261.553		
1	2	177.778	-22.148	179.152	5.464	10.524
1	3	83.221	5.127	83.378	2.808	7.085
2	2	18.300	36.122	40.493		
2	1	-172.314	32.671	175.384	5.464	10.524
2	4	45.712	2.705	45.792	1.106	-0.517
2	5	82.990	1.703	83.008	2.995	8.178
2	6	61.912	-0.958	61.920	2.048	2.264
3	3	-2.400	-1.200	2.683		
3	1	-80.412	1.958	80.436	2.808	7.085
3	4	**78.012**	-3.158	78.076	0.771	1.344

The TCSC is used to raise the amount active power flowing from bus3 towards bus4 to a higher value of 100MW instead of 78.012MW, that is an increase of about 28%. This is done by creating a new bus (31) between bus3 and bus4 to connect the TCSC between bus3 and bus31 so that the active power flowing towards bus4 is the specified regulated power i.e. 100MW. The model manages to maintain the specified active power flowing towards bus4 in seven iterations with a final firing angle of 143.7995° as shown in table (6).

Table (6): Power flow results of 30-bus system with TCSC connected
For bus 3 only

Line Flow and Losses						
--Line--		Power at bus & line flow			--Line loss--	
From	To	P(MW)	Q(MVAR)	S(MVA)	P(MW)	Q(MVAR)
3	3	-2.400	-1.200	2.683		
3	1	-102.400	17.773	103.931	4.607	14.405
3	31	100.000	-18.973	101.784	0.000	-8.617
4	4	-7.600	-1.600	7.767		
4	2	-34.364	-7.698	35.216	0.676	-1.827
4	31	-98.721	13.161	99.594	1.279	2.806
4	6	80.593	-21.523	83.418	0.806	1.882
4	12	44.892	14.460	47.163	0.000	4.828
31	31	0.000	0.000	0.000		
31	3	-100.000	10.355	100.535	0.000	-8.617
31	4	100.000	-10.355	100.535	1.279	2.806
Total loss					17.704	15.574

To test weather the new system has acquired a new margin for transient stability, a three phase fault is created near bus1 at transmission line (1-3), and removed by the removal of the same transmission line for both the base case and the new system with the TCSC connected. For the model without the TCSC connected, when the faulty line was cleared, and after a clearing time Tc of 0.224sec, the swing curve shows that the power angle returns after a maximum swing, and loses its stability for a clearing time of Tc=0.225sec. Hence, the system is found to be stable for CCT=0.224sec, as shown in Figure (8).

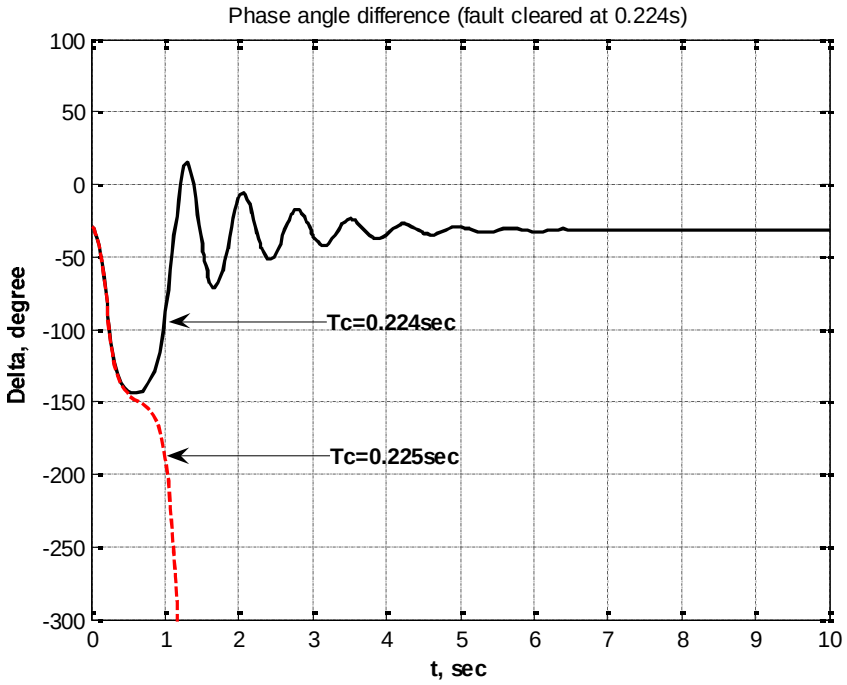

Figure (8): Power angle curve for IEEE30-bus test system, fault at T.L. 1-3 Without TCSC included

As the active power in the branch where the TCSC is connected has been enhanced, it is now time to check for the enhancement of transient stability. The same procedure for fault created near bus1 at transmission line 1-3 for the base case, is simulated and the power angle difference is plotted in Fig. (9). The power system is seen stable for CCT=0.226sec, the system has gained an increase in stability margin of 0.8% as compared to the base case.

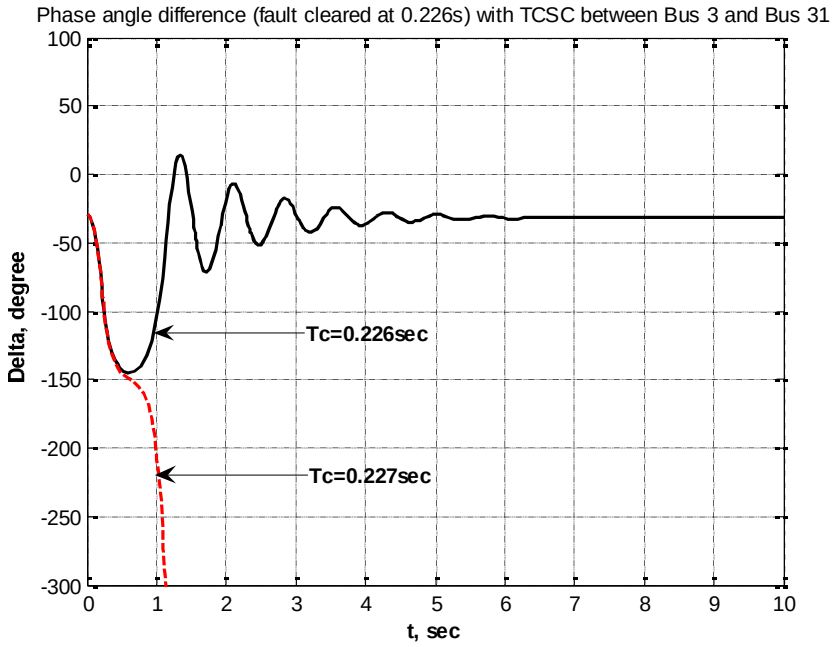

Figure (9): Power angle curve for 5-bus test system, fault at T.L. 1-3 With TCSC included

5. Conclusion:

In this paper the model for power flow and transient stability for an IEEE five and an IEEE thirty bus test systems was developed and the resultes for specifying the active power flow in a certain branch of the power system was verified, the transient stability was also tested and the results show that the stability margin was increased by 0.5% and the power flow by 8.33% for the 5-bus test system, and by 0.8% for the stability margin and 28% for the power flow in the 30-bus power system when the TCSC device was connected.

References:

1. D. Karlsson and S. Lindahl, "Wide area protection and emergency control," in Proc. IEEE Power Eng. Soc. General Meeting, vol. 1, 2004, p.5.
2. F. F. Song, T. S. Bi, and Q. X. Yang, "Study on wide area measurement system based transient stability control for power systems," in Proc. IPEC Power Engineering Conf., vol. 2, 2005, pp. 757–760.
3. A. G. Phadke, "Synchronized Phasor Measurements in Power Systems," IEEE Computer Appl. Power, Vol. 6, No. 2, Apr. 1993, pp. 10–15.
4. H. Dongchen and V. Venkatasubramanian, "New Wide-Area Algorithms for Detection and Mitigation of Angle Instability Using Synchrophasors," in Proc. Power Eng. Soc. General Meeting, June 2007, pp. 1–8.
5. P. Kundur, 1. Paserba and V. Ajjarapu , " Definition and Classification of Power System Stability IEEE/CIGRE Joint Task Force on Stability Terms and Definitions," IEEE *Trans*. on *Power Systems*, Vol. 19, Aug. 2004, pp. 1387-1401.

6. M. Pavella, D. Ernst, D. Ruiz-Vega, “Transient Stability of Power Systems,” Kluwer Academic Publishers, 2000, p. 6.
7. A. Olwegard, K. Walve, G. Waglund, H. Frank, S. Toresng, “Improvement of transimission capacity by thyristor controlled reactive power,” IEEE Trans. On Power Apparatus and Systems, Vol. 100, No. 8, 1981, pp. 3930-3939.
8. P. Poubeik, P. S. Kundur, C. W. Taylor, “The anatomy of a power grid blackout,” IEEE power & energy magazine, Sep/Oct 2006, pp. 22-29.
9. L. Wehenkel, M. Pavella, “Preventive vs. Emergency Control of Power Systems,” IEEE/Power Energy Society Power Systems Conference & Exposition, Vol.3, 2004, pp. 1-6.
10. D. Ernst, L. Wehenkel, M. Pavella, “What is the likely future of real-time transient stability?” IEEE Power Energy Society Power Systems Conference and Exposition, 2009,pp.1-3.
11. Xu Yanhui, Si Dajun, Qian Yingchun, "Effect of Load Model on Yunnan Power Grid Transient Stability" IEEE Power and Energy Engineering Conference , 2011, pp.1-4.
12. Ayman Hoballah, and István Erlich, Senior Member, IEEE," Transient Stability Assessment using ANN Considering Power System Topology Changes" IEEE 15th International Conference on Intelligent System Applications to Power Systems, 2009, pp. 1.
13. N.G. Hingorani, L. Gyugyi, “Understanding FACTS: Concepts and Technology of Flexible ac Transmission Systems”, Wiley-IEEE Press, New York, 2000.
14. Kirschner L.; Retzmann D.; Thumm G.;” Benefits of FACTS for Power System Enhancement”, Transmission and Distribution Conference and Exhibition: Asia and Pacific, 2005 IEEE/PES, pp.1 – 7.
15. Mohammed Osman Hassan, S. J. Cheng, Senior Member, IEEE, Zakaria Anwar Zakaria," Steady-State Modeling of SVC and TCSC for Power Flow Analysis"Proceedings of the International MultiConference of Engineers and Computer Scientists 2009 Vol II IMECS 2009, March 18 - 20, 2009, Hong Kong
16. M.Kowsalya1, K.K.Ray1, and D.P.Kothari2 1 VIT University /School of Electrical Engineering, PED Division, Vellore, India"Positioning of SVC and STATCOM in a Long Transmission Line" International Journal of Recent Trends in Engineering, Vol 2, No. 5, November 2009.
17. Enrique Asha, Claudio R. Fuerte Esquival, Hugo ambriz, and Cezar Angeles-Camacho, "Modeling and simulation in Power Networks" John Wiley & Sons Ltd, The Atrium, Southern Gate, Chichester, 2004.
18. Hadi Saadat "Power System analysis", McGraw-Hill Series in Electrical Computer Engineering, 1999.